Journal of Fluorescence, Vol. 9, No. 3, 1999

Ab Initio Study of the Phosphorescence of Nitrite Ions

B. F. Minaev[1] and V. A. Minaeva[2]

Received October 6, 1998; accepted December 8, 1998

In order to interpret the phosphorescence spectra of $NaNO_2$ and similar single crystals, we performed MCSCF geometry optimization in the ground singlet (X^1A_1) and in the first excited triplet (a^3B_1) states of the NO_2^- ion and MCSCF quadratic response (QR) calculation of the a^3B_1–X^1A_1 transition probability at different bending angles and asymmetric stretch modes. The complete form of the spin–orbit coupling (SOC) operator is accounted for in the QR procedure. Dunning's correlation-consistent polarized valence double-ζ (cc-pVDZ) and triple-ζ (cc-pVTZ) basis sets are imployed. The electric-dipole transition moment from the T^z spin sublevel (z is the C_2 axis) oriented along the y direction (the other in-plane axis) is found to be $\simeq$5 times higher than that from the T^y sublevel in the ground-state geometry. This is in agreement with polarization measurements and with optical detection of ESR spectra. The T^z–S_0 transition moment decreases almost linearly with an increase in the ONO bond angle. The so-called non-Condon effects in the phosphorescence spectra of $NaNO_2$ crystals are explained on these backgrounds. The long progression of the bending vibrations (ν_2, a_1) with an anomolous intensity distribution in the T^z–S_0 transition and additional involvement of the asymmetric stretch mode (ν_3, b_2) in the T^y–S_0 transition are interpreted by force field and SOC calculations in the MCSCF-response technique. Configuration interaction (CI) calculations of the spin-allowed electric dipole transitions in NO_2^- ions with effective one-electron SOC operator matrix element estimations were done for comparison with the results of the quadratic and linear response methods. Other T_n–S_0 transitions are also studied. Finally, a short discussion of nonradiative processes is presented.

KEY WORDS: Phosphorescence; nitrite ions; *ab initio* study.

INTRODUCTION

The Jablonski diagram provided a successful attempt to rationalize various intra- and intermolecular processes initiated by photon absorption in organic solvents, glasses, and crystals [1]. The famous three-level diagram with a metastable *P* term (which latter was assigned as a triplet state [2,3]) explained the strong phosphorescence of solid and viscous solutions of many organic compounds and, also, the delayed fluorescence [1]. At the begining of the thirties it was not yet realized that many photophysical processes in organic molecules are controlled by violations of spin selection rules induced through spin–orbit coupling (SOC). SOC determines a mixing between the singlet (S) and triplet (T) states and is relatively weak in molecules consisting of first-row atoms. So the total electronic spin is still a good quantum number and the degree of violation of spin-forbiddness is small. Nevertheless, nonradiative and radiative S–T transitions occur at a competitive rate in light molecules and phosphorescence ($T_1 \rightarrow S_0$ emission) is a common feature of molecular afterglow [2,3]. Electron spin resonance (ESR) studies of triplet excitons and triplet traps in organic crystals provided final support for the modern version of the Jablonski diagram [3].

In single crystals of $NaNO_2$ there exists a metastable triplet (T_1) state whose spectroscopic properties are similar to those of triplet excitons in organic molecular crys-

[1] Cherkassy Engineering and Technological Institute, 257006, Cherkassy, Ukraine.
[2] Cherkassy State University, 257001, Cherkassy, Ukraine.

1053-0509/99/0900-0221$16.00/0

tals [4,5]. The T_1 state properties of neat $NaNO_2$ and of some doped crystals have attracted great attention for two decades (see, e.g., Refs. 6–8), since the first measurement of nitrite anion phosphorescence in 1968 [4]. The trap triplet state in $NaNO_2/Ag^+$ and in other crystals as in neat $NaNO_2$ has been assigned to a $(n\pi^*)$-type excitation localized on the NO_2^- anion [4,7,8]. The crystal structure of $NaNO_2$ is particularly attractive for Zeeman effect studies since all nitrite anions are similarly oriented with their symmetry axes parallel to the crystal axes [5–7,9].

Though there are some semiempirical calculations of SOC effects in nitrite anions (NO_2^-) [6,10–13], it is of interest to make direct *ab initio* calculations of the phosphorescence radiative lifetime, which are now possible with the modern quadratic response techique [14]. This is the main goal of the present paper. Since the first SCF MO CI study [10] of SOC effects on the optical and ESR spectra of nitrite ions, there have been some similar CI calculations of vibronic perturbation [12] and of the metal-cation influence on nitrite ion phosphorescence spectra [11,13]. Semiempirical calculationss of SOC integrals in NO_2^- ions published in Refs. 6 and 10 are rather contradictory. It would be interesting to compare these old results with modern *ab initio* calculations of SOC integrals, since the response technique produces very reliable SOC energy splittings [14].

The low-lying electronic states of the nitrite anion have been studied by numerous researchers both theoretically [6,10,11,15–17] and experimentally [6,11,18–25]. The near-ultraviolet absorption spectra of NO_2^- in different solvents [18] and in crystals [6,19,23,26] have been interpreted as weak singlet–singlet (S–S) transitions of $\pi^* \leftarrow n$ nature (weak bands near 360 and 280 nm are assigned as $^1B_1 \leftarrow {}^1A_1$ and $^1A_2 \leftarrow {}^1A_1$ absorption, respectively [17,18]). The intense band near 210 nm was interpreted as belonging to a $^1B_2 \leftarrow {}^1A_1$ transition of $\pi^* \leftarrow \pi$ nature. In neat alkali metal nitrite crystals [6,26] and in alkali halide hosts [20–22], a strong fluorescence $^1B_1 \rightarrow {}^1A_1$ was observed at low temperatures. In neat $NaNO_2$ and in some doped crystals a very weak phosphorescence $^3B_1 \rightarrow {}^1A_1$ has been studied by different methods in many details [6,11,19,24] including ESR [5] and optical detection of magnetic resonance (ODMR) [7,23,25] measurements. The transition energy and polarization are in good agreement with theoretical results [10,15]. So the assignment of all spectroscopically observed low-lying electronic states of the nitrite anion is well determined. Only vertical transitions from the ground state have been calculated before [10,15–17]. Tinti *et al.* [7,23] have found anomalous intensity distributions for the totally symmetric bending progression in phosporescence spectra of NO_2^- in $NaNO_2$ and $NaHCO_2$ crystals and called these phenomena non-Condon effects. In the following an *ab initio* version of the previous CNDO/S CI interpretation [10] of the SOC effect on spin-selective phosphorescence $^3B_1 \rightarrow {}^1A_1$ of nitrite ions is given, with special attention to the non-Condon effect explanation.

METHOD OF CALCULATIONS

In previous work [10] the first-order perturbation theory treatment of the SOC effect on the singlet–triplet (S–T) transition probability [3] has been used. In this approach the SOC perturbation is described in terms of a selected set of intermediate S and T states and the S-T transition probability is borrowed from the spin-allowed S–S and T–T transitions. The S_0–T_1 transition dipole moment is determined in this case performing explicit summations over the intermediate states:

$$\langle S_0^1|r^l|T_1^{k,1}\rangle = \sum_n \frac{\langle S_0^0|r^l|S_n^0\rangle \langle S_n^0|H_{so}^k|T_1^{k,0}\rangle}{E(T_1^0) - E(S_s^0)} + \sum_m \frac{\langle T_m^{k,0}|H_{so}^k|S_0^0\rangle^* \langle T_m^{k,0}|r^l|T_1^{k,0}\rangle}{E(S_0^0) - E(T_m^0} \quad (1)$$

where H_{so}^k is the kth component (k, $l \in x$, y, z) of the SOC operator (the superscript indices 0 and 1 denote the order of perturbation theory). The x, y, and z axes are connected with the molecular frame and are main axes of the zero field splitting (ZFS) tensor [3]. The triplet-state spin sublevels T^k are split by weak intramolecular magnetic interactions: by spin–spin coupling in the first order of the perturbation theory and by SOC in the second order [10]. Each spin sublevel has its own S_0–T_1^k transition probability, which makes possible the optical detection of magnetic resonance (ODMR) even in a zero external magnetic field for crystals at low temperatures ($\leq$4.2 K) when the spin-lattice relaxation is frozen [5,10,23]. The ZFS spin functions are related to the high external magnetic field spin functions (ordinary $M_s = 0$; ± 1 spherical components) by

$$T^z = \frac{T^{-1} - T^1}{\sqrt{2}}, \qquad T^y = i\frac{T^{-1} + T^1}{\sqrt{2}}, \qquad T^z = T^0 \quad (2)$$

In this spin basis we have simple relations, $S^kT^k = 0$, $S^xT^y = iT^z$, etc., where S^x is the total spin projection operator on the x-axis, $\langle S_n|H_{so}^k|T_m^k\rangle = \langle T_m^k|H_{so}^k|S_n\rangle^*$. The second sum in Eq. (1) has often been neglected [3], supposing that the ground singlet state of diamagnetic molecules has no appreciable triplet-state admixtures. Such truncation of row (1) was revealed to be a bad approxima-

tion; calculations [10,14,27] showed that the second term in Eq. (1) is very important; the T–T transitions often produce a larger contribution to the phosphorescence rate constant than the S–S transitions. In the restricted configuration interaction (CI) method, row (1) was shown to converge very slowly [14,27,28]. Highly excited states with a large energy denominator in integral (1) make appreciable contributions because of the stronger SOC between these far-separated S and T states for a large variety of aromatic molecules [28,29]. Langhoff and Davidson [27], in their CI study of H_2CO, noted that in order to obtain a converged S–T transition moment for formaldehyde, it was not sufficient to include the lowest 100 states in S and T manifolds. Many terms in sum (1) are of similar magnitude but of different signs. The restricted CI method also leads to size-consistency errors when the S–T transition moment dependence on vibrational coordinates is studied. Different geometries of the same molecule can lead not only to different sets of configuration wave functions, but also to different patterns of summation in the truncated row (1).

Instead of the sum-over-state expression (1) for the S–T transition moment Vahtras *et al.* [30] used an alternative approach, namely, the response theory, and demonstrated that the matrix element of Eq. (1) is associated with the residue of a quadratic response function [14],

$$\lim_{\omega\to\omega_1} (\omega - \omega_1) \langle\langle r^l; H^k_{so}, C\rangle\rangle_{0,\omega} \qquad (3)$$

where C is an arbitrary triplet operator. Vahtras *et al.* [30] have shown how this S–T transition dipole moment can be calculated with the multiconfigurational quadratic response (MCQR) method as employed in the present work. At the multiconfigurational self-consistent field (MCSCF) level of theory, the response method employs the operators associated with orbital—and CI—relaxation to describe the effect of an external perturbation [14]. The method is fully analytic, *i.e.*, an analytic analogue of a finite field perturbation from an MCSCF linear response calculation where the SOC operator represents the applied field [14]. By allowing the orbitals to relax in the response to the external field, the requirements for the CI expansion are reduced. Conventional CI approaches use only configuration excitation operators and more extensive calculations are therefore required in such approaches in order to obtain an equal correlation level. MCSCF response theory has successfully described linear and nonlinear optical and magnetic properties [14,31] employing rather modest MCSCF expansions. The sum-over-state expression (1) in MCQR theory of the S–T transition moment is replaced by solutions of sets of linear equations [30]. Since these solutions can be determined using direct iterative techniques of the response equations, large dimensions and therefore large orbital and configuration space MCSCF wave functions can be considered. So errors from truncation of the slowly convergent summations, employed in conventional procedures, are completely avoided.

In this paper calculations of spectral properties of the NO_2^- anion have been performed in different basis sets and complete active spaces (CAS), accounting for linear and quadratic MC (multiconfiguration) response functions with the DALTON code [32]. A full form of the SOC operator [14], including one- and two-electron terms, is employed. The choice of axes is given in Fig. 1. The Dunning [33] correlation-consistent polarized valence double-ζ (cc-pVDZ) basis set was used for all geometry-dependent calculations. Basis sets of Ahlrichs *et al.* [34] and the Dunning triple-ζ (cc-pVTZ) basis set are also used for comparison. In the equilibrium ground-state 1^1A_1 geometry the Hartree–Fock electronic configuration of nitrite anions is

$$1^1A_1 = (\text{core})^{12}\,(5a_1)^2\,(3b_2)^2\,(1b_1)^2\,(4b_2)^2\,(1a_2)^2\,(6a_1)^2\,(2b_1)^0 \qquad (4)$$

The core orbitals, besides three inner shell AOs, include two MOs ($3a_1$, $2b_2$) with a low energy (about -1 a.u.) and the highest orbital ($4a_1$) with an energy of -0.63 a.u. These core MOs were inactive in almost all MCSCF calculations presented in this paper. All other six occupied MOs and three empty MOs ($2b_1$, $5b_2$, $7a_1$) have been included in the MCSCF calculations (12 electrons in 9 orbitals): CAS (3,2,3,1) corresponding to the standard order of irreducible representations of the C_{2v} group (a_1, b_1, b_2, a_2). Inclusion of the occupied valence orbital ($4a_1$ MO) with a low energy (-0.63 a.u.) has practically no influence on the results of spectral calculations. Calculations with this CAS (4,2,3,1) were done only in the ground-state equilibrium geometry and are discussed here very briefly (Table III). Extension to a very large CAS (4,2,4,2), which includes 213,840 determinants, has been studied in both the singlet ground-state and the triplet-state equilibrium geometry and found to produce a minor

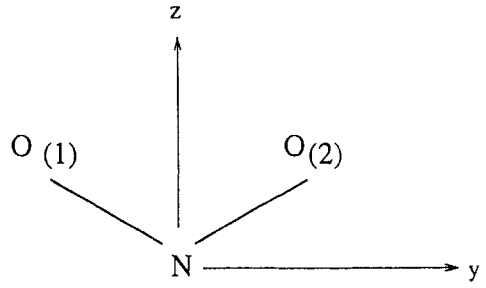

Fig. 1. Choice of axes for the NO_2^- molecule.

change in phosphorescence radiative lifetime (Table III). So almost all MCQR calculations were performed in a moderate CAS (3,2,3,1) with 12 active electrons distributed in 9 MOs.

RESULTS OF CALCULATIONS AND DISCUSSION

The results of our MCSCF geometry optimization in the ground and in the first excited triplet state of the NO_2^- molecule together with other theoretical and experimental data are presented in Table I. For the ground state all methods (excepting the basis sets of Ahlrichs *et al.* [34]) predict similar results which are quite close to the experimental data [16] and to the recent coupled cluster CCSD(T) calculations [15]. All our calculations predict the bond angle ∠ONO to be about 115.9°, in close agreement with the experimental values of 115.4° [16] and 116° [9]. In the phosphorescent T_1 state (1^3B_1) the bond angle ∠ONO is increased by 15.5° from 115.4° in the gound state [7]. In the first excited singlet state, 1^1B_1 it encreases by 13.5° [7]. Our MCSCF geometry optimization in the cc-pVDZ basis set gives 14.83 and 12.98° for the bond angle ∠ONO increase in the triplet and singlet B_1 states, respectively. This demonstrate excellent agreement with analysis of the vibrational structure of the phosphorescence and fluorescence of NO_2^- ions in $NaNO_2$ and other crystals [6,7,35].

The basis sets of Ahlrichs *et al.* [34] overestimate bond lengths and predict low vibrational frequencies. The intensity ratio for the ν_1 (N–O stretch) and ν_2 (bend) vibrations is 1.74, 1.86, and 1.48 for the first three methods, presented in Table I. All infrared (IR) spectral intensities for the ground state correlate qualitatively with each other. The IR intensity of asymmetric stretch vibration in the triplet state quite differs in both methods presented in Table I. Obviously the basis sets of Ahlrichs *et al.* [34] are less reliable for molecular force field calculations. The IR spectrum of nitrite ions in the triplet excited state could be easily measured in flash photolysis experiment, since a high concentration of triplet ions can be achieved [11] and the gound-state IR spectrum is quite different from the triplet one.

The cc-pVDZ basis set gives geometry, vibrational frequencies, and IR intensities in good agreement with available experimental data. It is known that asymmetric stretch vibration in nitrite anions is very intensive in IR

Table I. Geometry Optimization for the Ground Singlet and First Excited Triplet States of the NO_2^- Molecule[a]

Method	r_{O-N} (Å)	∠NON (deg)	ν_1 (sym.) a_1	ν_2 (bend) a_1	ν_3 (asym.) b_2	E_n (Hartrees)
			Ground state, 1^1A_1			
cc-pVDZ[b]	1.2759	115.98	1322.1 (13.74)	788.5 (7.9)	1254.9 (481.1)	−204.223189
cc-pVTZ[b]	1.2699	115.97	1341.8 (12.1)	804.4 (6.5)	1251 (476.2)	−204.293076
Ahlrich's VTZ[b]	1.3352	115.36	1132.55 (15.1)	691.3 (10.2)	954.6 (548.5)	−204.227060
6–31 G(d)[b]	1.2789	115.86				−204.280657
CCSD(T)[c]	1.2638	116.41	—	—	—	−204.889420
CASSCF[c]	1.2691	116.32	—	—	—	−204.314746
(5s3p) diffuse, CI[d]	1.2359	115.4	—	—	—	−204.30041
Expt.[e]	1.2359	115.4	1330	829.7	1242	
			First excited triplet state, 1^3B_1			
cc-pVDZ[b]	1.3090	130.81	1009.6 (4.4)	592.4 (0.6)	1092.4 (285.3)	−204.116790
Ahlrich's VTZ[b]	1.3815	128.22	818.4 (3.9)	508.0 (0.23)	813.7 (60.8)	−204.113507
(5s3p) diffuse, CI[d]	1.2359	115.4	—	—	—	−204.20901
Exp.[f]	~1.29	130.9	—	646	—	
Expt.[g]	—	129 ± 2	1124	644	1170	

[a] r denotes the internuclear N–O distance (Å), and ν the vibrational harmonic frequency (cm^{-1}). IR intensities (km/mol) are given in parentheses. E_n is the total energy.

[b] This work. MCSCF CAS (3,2,3,1).

[c] Ref. 15. Augmented cc-pVTZ basis set of Dunning *et al.* [33] with the omission of the diffuse *f*-type functions is used. CAS (5,2,4,1); 18 electrons in 12 MOs.

[d] Ref. 16. Calculated in the ground-state experimental geometry.

[e] Geometry is cited in Ref. 16; vibrational frequency from Ref. 7.

[f] Ref. 7.

[g] Ref. 6.

spectra, in qualitative accord with our results (Table I). The changes of vibrational frequencies upon $S_0 \rightarrow T_1$ excitation are also well reproduced at the cc-pVDZ level in a small CAS (3,2,3,1). For example, the bending vibration frequency is reduced by 196 cm^{-1} in this method, whereas the experimental shift is 186 cm^{-1}. The method reproduces vertical excitation energies and intensities fairly well (Table II). So we use this method for the triplet-state property calculations by the response technique.

Asymmetric Stretch Potentials for Low-Lying States of NO_2^- Ions Obtained by the Linear Response MCSCF Method

The asymmetric stretch potentials for eight low-lying states of NO_2^- ions have been studied by linear response MCSCF calculations in CAS (3,2,3,1) with simple prolongation of one of the N–O bonds, keeping the rest of parameters fixed at their equilibrium position. This is not a proper reaction coordinate for dissociation of the molecule, but still the potentials simulate qualitative features of the photochemical behavior of different states. The results are shown in Fig. 2. The states of the A_1, B_2 orbital symmetry in the C_{2v} group correlate with the A' states in the distorted molecule (the C_s point group) and the symmetries B_1, A_2 correlate with the A'' states, respectively.

The lowest excited triplet and singlet states $^{3,1}B_1$ are found to be stable with respect to prolongation of one of the N–O bonds (Fig. 2). The triplet state, especially, is pretty stable and has a dissociation energy of about 1 eV; the singlet $^1B_1$ counterpart is less stable ($D_e \approx 0.46$ eV). Both states dissociate to the radical pair limit $O^-(^2P)$ + $NO(^2\Pi)$. The other two states of the A'' symmetry, the singlet and triplet terms, which originate from the $^{1,3}A_2$ states, are weakly bound; the singlet is more stable. Both potentials are very flat and demonstrate a tendency to reproduce a distorted NO^-_2 molecule with two different bond lengths (Fig. 2).

The $\pi\pi^*$ excited states of the A' symmetry are repulsive with respect to dissociation on NO^- + O. These are those states which originate from the $^3B_2$, 2^1A_1, and $^1B_2$ terms produced by vertical excitations from the ground state. The last potential, $^1B_2(3^1A')$, has a distinct local minimum at $R(NO_{(1)}) = 1.33$ Å when the other bond is fixed at the distance $R(NO_{(2)}) = 1.279$ Å (Fig. 2). The $(\pi-\pi^*)$ transition $1^1A_1 - {}^1B_2$ in the UV region of the spectra is the most intensive one (the oscillator strength, $f \simeq 0.12$; Table II). This is typical for spectra of other isoelectronic molecules (O_3, SO_2 SeO_2) which also demonstrate the asymmetric C_s distortion in the upper singlet $\pi\pi^*$ state [7, 28]. The $^3B_2(1^3A')$ state dissociates to the same $NO^-(^3\Sigma^-)$ + $O(^3P)$ dissociation limit as the ground state.

Finally, the qualitative potentials presented in Fig. 2 demonstrate the bonding character of the two triplet $n\pi^*$ states, $^3B_1$ and $^3A_2$. The lowest triplet $\pi\pi^*$ state, $^3B_2(^3A')$, is photochemically unstable (Fig. 2) and has a

Table II. Vertical Excitation Energies (eV) and Oscillator Strengths (in Parentheses) for the Singlet–Singlet and Singlet–Triplet Transitions of the NO_2^- Ion

State	cc-pVDZ[a]	cc-pVTZ[a]	6–31 G, CI[b]	CASSCF[c]	CI[d]	Expt.[e]
			S–S transitions			
$^1B_1$	3.40 (1.3×10^{-3})	3.46 (1.1×10^{-3})	3.12 (3.1×10^{-3})	3.83	3.43	3.5 (5×10^{-4}) [3.2]
$^1A_2$	4.31 (0)	4.35 (0)	4.97 (0)	4.44	4.18	4.2–4.3 (3×10^{-4})
$^1B_2$	6.33 (1.57×10^{-1})	6.18 (1.2×10^{-1})	6.74 (1.16×10^{-1})	6.58	—	6.0 (1.2×10^{-1})
2^1A_1	10.18 (5.6×10^{-2})	10.06 (5.1×10^{-3})	6.69 (3.5×10^{-4})	7.49	—	—
			S–T transitions[f]			
1^3B_1	2.45 (2.32×10^{-8})	2.47 (2.7×10^{-8})	2.11	2.94	2.58	2.9 [2.4] (8×10^{-8})[g]
1^3A_2	4.12 (2.08×10^{-6})	4.16 (3.11×10^{-6})	4.86	4.31	3.91	≈4.15[h]
1^3B_2	3.92 (4.4×10^{-10})	4.03 (3.11×10^{-10})	4.52	4.31	3.75	—

[a] This work. Linear response from MCSCF CAS (3,2,3,1).
[b] This work. CI in CAS (3,2,3,1).
[c] Ref. 15. See Table I, footnote *c*.
[d] Ref. 16. [5s3p] diffuse basis.
[e] Experimental data from Ref. 17; the 0–0 transition energy is given in brackets.
[f] Oscillator strengths for the S–T transitions are calculated by the MCQR method.
[g] Ref. 6.
[h] Ref. 7.

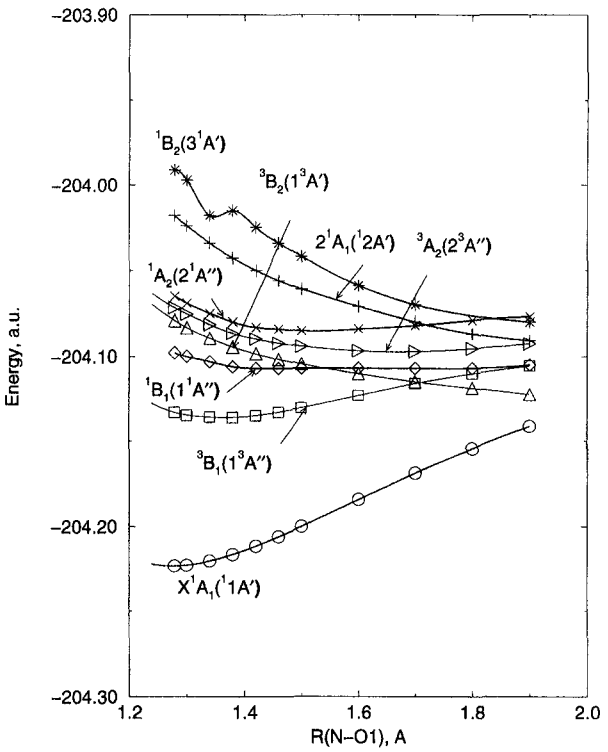

Fig. 2. N–O_1 bond length dependence of the total energies for the ground and the few lowest excited singlet and triplet (thin lines) states in the NO_2^- molecule calculated by the MCSCF LR method in the cc-pVDZ basis set. The N–O_2 bond is fixed at R = 1.279 Å; bond angle ONO = 116°.

negligible oscillator strength for the vertical transition from the ground state as follows from our MCQR calculations (Table II). This state could not be observed directly in absorption, but it probably influences indirectly the fluorescence of nitrite ions (see discussion in the last section).

Bending Potentials for Low-Lying States of NO_2^- Ions Obtained by the Linear Response MCSCF Method

Both the fluorescence and the phosphorescence of NO_2^- anions in different host crystals are accompanied by a long progression in the symmetric bending mode ($\nu_2'' \simeq 830$ cm^{-1}). A similar progression also occurs in the corresponding absorption spectra ($\nu_2' \simeq 640$ cm^{-1}) [4,6–8,19,22,24,26]. This implies large changes in the ONO bond angle, ~14 ± 2° [6], during the $^3B_1$–$^1A_1$ and $^1B_1$–$^1A_1$ transitions [7, 24]. As mentioned before, our MCCSF calculations with complete geometry optimization reproduce this behavior pretty well (Table I). Similar results are obtained by the linear response MCSCF method in the same CAS (3,2,3,1) with the ONO angle variation at fixed N–O bond lengths, R(N–O) = 1.279 Å. The potentials are presented in Fig. 3 for the three lowest triplet excited states together with the ground-term curve (MCSCF). The $^3B_1$ state has a minimum at 133.6°, the $^3A_2$ state at 97.4° and the $^3B_2$ state is bent at 109.9°. The last value is the closest to the ground-state equilibrium (116°). Similar results are obtained for the singlet excited state bending potentials. The $^1B_1$ state has a minimum at 131.1°; the $^1A_2$ state, at 98.5°. The bending in the $^1B_2$ state is almost the same as in the triplet counterpart at the fixed bond lengths. We have not studied the complicated hypersurface of the last state in more detail but we can say that it is characterized by avoided crossings of a number of configurations with different behavior with respect to asymmetric and symmetric stretchs. It probably has two local minima.

Other studied potentials are rather smooth. We can conclude from Fig. 3 that the $^3B_1$ bending potential is characterized by a high anharmonicity. It is crossed by the ground-state potential at an ONO angle of 150° and this behavior should be responsible for phosphorescence nonradiative quenching. We discuss the potentials shown in Figs. 2 and 3 in connection with nonradiative processes considered in Section 3.5.

Spin-Selective Radiative Transitions in the $^3B_1$–1^1A_1 System

The $^3B_1$–1^1A_1 system of nitrite ions has been studied in both absorption and emission for a number of host crystals [7, 24]. The oscillator strength (f) for the $^3B_1 \leftarrow 1^1A_1$ absorption was also measured from a solution spectrum ($f = 8 \times 10^{-8}$) [6]. About 90% of the absorption intensity in crystals was observed when the light was polarized along the b crystallographic axis, that is, the y axis in Fig. 1. The other 10% was found in the a spectrum (the z polarization in Fig. 1) [6]. The unique polarization of the $^3B_1$–1^1A_1 transition suggests that only one spin sublevel of the triplet state can undergo an efficient electric–dipole connection with the ground singlet state.

The triplet-state spin sublevels, Eqs. (2), transform as irreducible representations of rotations around the symmetry axes; in the C_{2v} point group they belong to the following symmetry:

$$T^x \in B_2, \qquad T^y \in B_1, \qquad T^z \in A_2 \tag{5}$$

The electric dipole moment ($M = e\Sigma_i r_i$) transforms as a translation along the axes:

$$M_x \in B_1, \qquad M_y \in B_2, \qquad M_z \in A_1 \tag{6}$$

The total spin–orbit symmetry of the $^3B_1$-state spin sublevels is

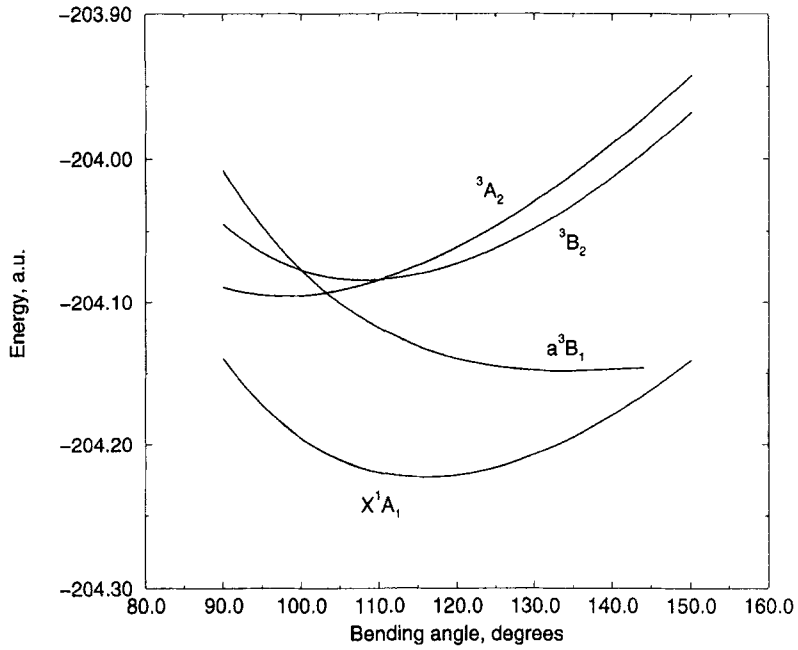

Fig. 3. Bending angle dependence of the total energies for the ground and the two lowest excited triplet states in the NO_2^- molecule calculated by the MCSCF LR method in the cc-pVDZ basis set.

$$T^x \in B_1 \otimes B_2 = A_2, \qquad T^y \in B_1 \otimes B_1 = A_1, \qquad T^z \in B_1 \otimes A_2 = B_2 \tag{7}$$

So we have the following selection rules for the $^3B_1$–1^1A_1 transition.

I. Transition to the x spin-sublevel of the triplet state is forbidden in electric dipole approximation even with the SOC account.

II. Transition to the y spin sublevel of the triplet state is z polarized (z is the in-plane C_2 axis; Fig. 1). We should remember that the y spin sublevel of the triplet state has a zero spin projection on the y axis, so both nonpaired spins are processing in the xz plane.

III. Transition to the z spin sublevel also has in-plane polarization but along the y axis. This is the strongest transition which was observed in crystals [6]. The molecular symmetry axes shown in Fig. 1 diagonalize the zero-field splitting (ZFS) Hamiltonian, which accounts for intramolecular magnetic interactions—spin–spin coupling and SOC [10]. They also coinside with the crystallographic axes.

The $^3B_1(T^z)$–1^1A_1 Transition

From the above analysis we see that the most intensive $^3B_1$–1^1A_1 transition is connected with the T^z spin sublevel and has y-polarization. This conclusion follows from the high-field Zeeman-effect measurement [6] and from the ODMR spectra [7,23–35].

A very simple MO study [6] with account of SOC mixing between the $^3B_1^z$ and the $^1B_2$ states,

$$\langle {}^3B_1^z | H_{soc}^z | {}^1B_2 \rangle \tag{8}$$

and intensity borrowing only from one S–S transition $^1B_2 - 1^1A_1$ at 210 nm (6 eV),

$$\langle 1^1A_1 | M_y | {}^3B_1^z \rangle = \langle {}^1A_1 | M_y | {}^1B_2 \rangle \frac{\langle {}^3B_1^z | H_{soc}^z | {}^1B_2 \rangle^*}{E(^3B_1) - E(^1B_2)} \tag{9}$$

seems to explain the main feature of nitrite ion phosphorescence, when integral (8) was estimated to be 35 cm^{-1} [6]. (All SOC integrals given in this paper are imaginary; the symbol $i = \sqrt{-1}$ is omitted for shortening.) The SCF CI calculations in the CNDO/S approximation [10] had shown that one term account in the sum of Eq. (1) is not sufficient: the SOC integral (8) is not as big as that obtained in a simple MO study [6]; it is only 11.8 cm^{-1} [10]. (We must remember that the square of the SOC integral comes to the transition probability.) Our calculation of this integral by the GAMESS program [36,37] with the effective nuclear charge, $Z_{eff}(N) = 4.55$ and Z_{eff} (O) = 5.6, for the one-electron SOC approximation [37] in Dunning's TZV basis set [38] and with CI in the same CAS (3,2,3,1), gives an even smaller value, 3.2 cm^{-1}, in the equilibrium singlet ground-state geometry

(∠ONO = 115.86°, R(N–O) = 1.279 Å, as determined by MCSCF geometry optimization in the TZV basis set). This SOC integral, Eq. (8), does not change much upon bond angle and bond length variations: it is 6.5 cm^{-1} in the equilibrium T_1-state geometry (∠ONO = 130.5° R(N–O) = 1.3127 Å, as determined by MCSCF geonetry optimization in the TZV basis set). So the value of the SOC integral, Eq. (8), calculated by Hochstrasser and Marchetti with simple wave functions is greatly overestimated. The obvious reason for this overestimation is connected with the fact that the wave function of the $^1B_2$ state is not simply described by a singly excited configuration $1a_2 \rightarrow 2b_1$ (as proposed in Ref. 6). This configuration produces the largest contribution (75%), but the $^1B_2$ state has some biradical character and also includes the doubly excited configurations $1b_1\ 1a_2 \rightarrow 2b^2_1$ (12%) and $1a_2\ 6a_1 \rightarrow 2b_1\ 7a_1$ (1%); other singly excited configurations are important as well: $4b_2 \rightarrow 7a_1$ (6%) and $6a_1 \rightarrow 7b_2$ (3%). Thus the SOC integral (8) is much smaller than proposed before [6] and the intensity borrowing term (9) cannot explain the observed phosphorescence rate constant.

There is another important contribution to the 1^1A_1–$^3B^z_1$ transition probability determined by the SOC integral [10]:

$$\langle {}^3A^z_2|H^z_{soc}|1^1A_1\rangle \qquad (10)$$

This integral is calculated by the linear response (LR) method with the complete form of the Breit–Pauli SOC operator [14] from the MCSCF CAS (3,2,3,1) wave functions in the cc-pVDZ basis set. It is presented in Fig. 4 as a function of the bending ONO angle. In the ground-state geometry the integral (10) is pretty large (58.3 cm^{-1}) and decreases with the bond angle enlargement, so at the T_1-state equlibrium it is 46.2 cm^{-1}. The corresponding values calculated by the GAMESS program are 56.0 and 45.9 cm^{-1}, respectively, which gives credit to the one-electron SOC approximation [37]. This contribution to the 1^1A_1–$^3B^z_1$ transition moment is equal to

$$\langle 1^1A_1|M_y|^3B^z_1\rangle = \langle {}^3B_1|M_y|{}^3A_2\rangle \frac{\langle {}^3A^z_2|H^z_{soc}|1^1A_1\rangle}{E(1^1A_1) - E({}^3A_2)} \qquad (11)$$

The T_1–T_3 transition moment is quite large,

$$\langle {}^3B_1|M_y|{}^3A_2\rangle = 0.495\ a.u. \qquad (12)$$

in the TZV CI method. Though this integral is smaller than the S_0–S_3 electric dipole transition moment,

$$\langle 1^1A_1|M_y|{}^1B_2\rangle = -0.938\ a.u. \qquad (13)$$

both contributions to the 1^1A_1–$^3B^z_1$ transition probability, Eqs. (9) and (11), are appreciable. The second term, Eq. (11), is about three times larger than the S–S contribution, Eq. (9), because of the weak SOC mixing determined by Eq. (8) and despite the large S–S transition dipole moment, Eq. (13). From that qualitative analysis we can predict that the T^z_1–S_0 transition moment, Eq. (11), should decrease with an increase in the ONO bond angle since the SOC integral, Eq. (10), in the numerator diminishes (Fig. 4) and the energy difference in the denominator rises (Fig. 3).

Direct calculations of the transition moment $M_y = \langle 1^1A_1|M_y|^3B^z_1\rangle$ by the MCQR method (Fig. 5) supported

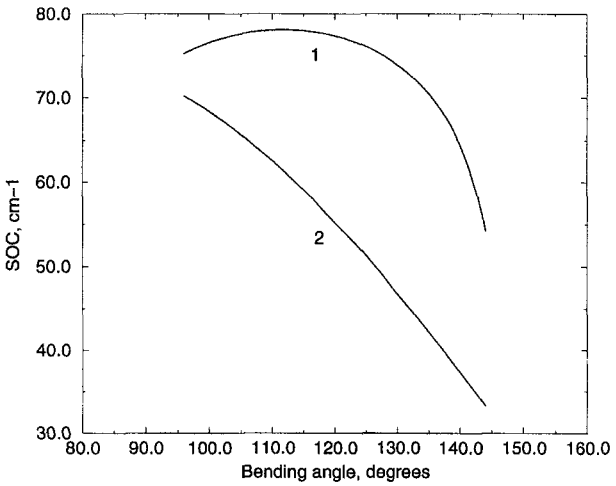

Fig. 4. Bending angle dependence of the SOC matrix elements between the ground and the excited triplet states in the NO_2^- molecule calculated by the MCSCF linear response method in the cc-pVDZ basis set. Curve 1: $\langle 1^1A_1|H_{soc}|{}^3B_1(T^y)\rangle$. Curve 2: $\langle 1^1A_1|H_{soc}|{}^3A_2(T^z)\rangle$.

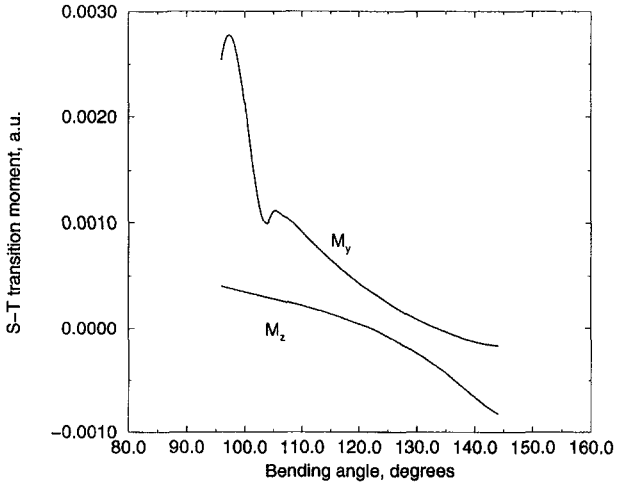

Fig. 5. Bending angle dependence of the transition dipole moments between the ground and the lowest excited triplet states $^3B_1$ for the T^z (M_y, light polarization along the y axis) and T^y (M_z, light polarization along the z axis) spin sublevels in the NO_2^- molecule calculated by the MCSCF quadratic response method in the cc-pVDZ basis set.

this qualitative conclusion. About 2000 contrbutions are taken into account in the MCQR calculations; the most important of them seems to be the term in Eq. (11). The calculated vertical $^3B_1 \leftarrow 1^1A_1$ transition moments for the T_z and T_y spin sublevels are presented in Table III. The oscillator strengths for the $T_1 \leftarrow S_0$ absorption (and for the other $T_n \leftarrow S_0$ transitions) are given in Table II.

From Fig. 5 it follows that the transition moment $M_y = \langle 1^1A_1|M_y|^3B_1^y\rangle$ decreases almost-linearly in the most important region of the ∠ONO angle variation, from 106 till 138°. The value M_y becomes zero at ∠ONO = 134.2°, i.e., in the vicinity of the T_1-state equilibrium ∠ONO angle. After this point the M_y value becomes negative, so the quantity $|M_y|^2$ starts to increase but is still very small. This behavior of the M_y transition moment, which determines the most intensive T_1–S_0 component both in absorption and in emission spectra with y polarization of light, could be responsible for the so-called non-Condon effects in the phosphorescence spectrum and in the cold $T_1 \leftarrow S_0$ absorption of nitrite anions [7]. We shall not go into the details of anomalous intensity distributions for the progression of the totally symmetric bending mode (ν_2) associated with the T^z spin sublevel and refer readers to the paper by Gotberg and Tinti [7]. Those authors have shown that the non-Condon effects can be reasonably interpreted in terms of a linear dependence of the stolen transition moment on the totally symmetric coordinate of the bending mode. At the same time they mentioned that "the detailed mechanism causing this effective linear dependence is unclear" [7]. Our results could be complementary to the analysis by Gotberg and Tinti [7].

Table III. MCSCF Quadratic Response Calculations of the Vertical Triplet–Singlet Transition Moment $M_a(T^b) = \langle 1^1A_1|e\ \Sigma_i\ a_i|1^3B_1(T^b)\rangle$ (in 10^{-6} a.u.) at the Equilibrium Geometry in the Ground State r_{O-N} = 1.2788 Å, angle ONO = 116[a]

M_a (T^b)	cc-pVDZ	cc-pVDZ[b]	cc-pVDZ[c]	cc-pVTZ
M_z (T^y)	125	131	133	229
M_y (T^z)	607	629	611	608
k_z (T^y)	0.24	0.27	0.30	0.84
k_y (T^z)	5.76	6.08	6.11	5.96
Transition energy (eV) and radiative lifetimes (s)				
$\Delta E_{S,T}$	2.45	2.44	2.41	2.47
τ^z	4.17	3.70	3.32	1.19
τ^y	0.17	0.16	0.15	0.17
τ_{av}	0.50	0.47	0.45	0.44

[a] k is the Einstein coefficient (s^{-1}) for spontaneous emission polarized along the z axis; $\Delta E_{S,T}$ is the transition energy, τ_b is the radiative lifetime of the T^b spin sublevel, τ_{av} corresponds to the high-temperature ($T > 77$ K) limit.
[b] Extended CAS (4,2,3,1); 14 electrons in 10 MOs.
[c] Extended CAS (4,2,4,2); 14 electrons in 12 MOs.

The calculated oscillator strength in Table II corresponds to the vertical $T_1 \leftarrow S_0$ transition. It is about three times smaller than the f value measured in solution, which is natural because the $T_1 \leftarrow S_0$ absorption band system consists of the long vibrational progression. The most intensive is the vertical (5–0) transition, but other bands, (6–0), (4–0), (3–0), are only slightly less intensive [7], so they will make additional contributions to the f value.

From Table III it follows that the T_1–S_0 transition moments calculated by the MCQR method with different complete active spaces and in different basis sets are very close to each other. Extension of the CAS from the (3,2,3,1) type to the (4,2,4,2) type leads to a huge increase in computational time; the number of determinants increases from 1788 to 213,840 and the MCQR procedure becomes tremendously complicated. But the T_1–S_0 transition probability is pretty stable with respect to this extension. The basis set dependence is more sensitive, but only for the weak transition to the T^y spin sublevel, which determines z-polarization (Table III).

The $^3B_1(T^y)$–1^1A_1 Transition

In discussing this transition intensity and the ratio M_y/M_z, it is relevant to say that the other SOC integrals presented in Table V of Ref. 6 are also somewhat discrepant with the semiempirical [10] and with our *ab initio* results. For example, the SOC integral

$$\langle {}^3B_1^y|H_{SOC}^y|2^1A_1\rangle \tag{14}$$

estimated to be 7 cm^{-1} by Hochstrasser and Marchetti [6], was found to be much higher (34 cm^{-1}) in the CNDO/S method [10]. Our calculation by the GAMESS program with the effective nuclear charge method [37] in the TZV basis set produces even higher values, 59.4 and 61.3 cm^{-1}, in the equilibrium S_0- and T_1-state geometry, respectively. (CNDO/S calculations have been performed in the ground-state geometrical structure; the y and z axes are interchanged in a previous paper [10] in comparison with the present choice.) The integral (14) determines the $^3B_1^y$–1^1A_1 transition polarized along the z axis, which gives only 10% of the total intensity in crystal absorption. This contribution

$$\langle 1^1A_1|M_z|^3B_1^y\rangle = \langle 1^1A_1|M_z|2^1A_1\rangle \frac{\langle {}^3B_1^y|H_{soc}^y|2^1A_1\rangle^*}{E(^3B_1) - E(2^1A_1)} \tag{15}$$

is not very large since the 2^1A_1 state has a high energy (Table II) and the S_0–S_4 transition is not intensive. Besides this contribution there is another important term deter-

mined by the difference in the permanent dipole moments of the S_0 and T_1 states. In the case $n = 0$, $m = 1$, the SOC matrix elements in the numerators of both terms in Eq. (1) are equal to each other and a particular contribution from the permanent dipole moments of the S_0 and T_1 states occurs; since the denominators have different signs the contribution to the transition moment (1) is proportional to the difference in the permanent dipole moments of these two states. In NO_2^- ions such terms contribute only to the direction of the permanent dipole moment (z axis), and for the T^y spin sublevel,

$$\langle 1^1A_1|M_z|^3B_1^y\rangle = [\langle 1^1A_1|M_z|1^1A_1\rangle - \langle {}^3B_1|M_z|{}^3B_1\rangle]\frac{\langle {}^3B_1^y|H_{soc}^y|1^1A_1\rangle^*}{E({}^3B_1) - E(1^1A_1)} \quad (16)$$

The difference in the permanent dipole moments of the T_1 and S_0 states in NO_2^- ions is very small: $\mu(S_0) = -2.54$ D and $\mu(T_1) = -2.65$ D in the ground-state geometry. Both contributions from Eqs. (15) and (16) have opposite sign and tend to cancel each other out at some ONO angle (together with a big variety of small contributions from Rydberg states).

The vertical ${}^3B_1^y \leftarrow 1^1A_1$ transition intensity with z-polarization is very weak (Table III). The calculated ratio of the y- to z-polarization for such a vertical transition is twice that in experimental measurements [6, 26]. Account of the asymmetric stretch distortion will change the ratio since the difference in the permanent dipole moments of the S_0 and T_1 states will increase greatly and the term determined by Eq. (16) will rise. This should influence the involvement of the asymmetric stretch vibration $\nu_3(b_2)$ to spin-selective transitions.

Influence of the Asymmetric Stretch Mode on the Intensity of the $T_1 \leftarrow S_0$ System

Upon asymmetric distortion the NO_2^- ion belongs to the C_s point group. The ${}^3B_1$ state corresponds to ${}^3A''$ symmetry in this point group. We have calculated 26 geometrical structures in the C_s point group, varying the ONO angle and each N–O bond length. The main qualitative conclusions from this study can be formulated as follows.

I. Transition $1^3A'' \leftarrow 1^1A'$ to the x spin sublevel is now allowed and is x-polarized (the x-axis is perpendicular to the molecular plane). MCQR calculations show that this transition is still very weak. At $R(N–O_{(1)}) = 1.5$ Å (other parameters being the same as in the ground state), we get $M_x = 0.00011$ a.u., which corresponds to the radiative rate constant $k_x = 0.086\ s^{-1}$.

II. Transitions $1^3A'' \leftarrow 1^1A'$ to the y and z spin sublevels each have their particular in-plane polarization. The intensity of the $T_1–S_0$ transition to the T^y spin sublevel is strongly increased: $M_y(T^y) = 0.00060$ a.u., and $M_z(T^y) = 0.00041$ a.u. Transition to the T^z spin sublevel polarized along the y axis is still the most intensive: $M_y(T^z) = 0.00078$ a.u. [the $M_z(T^z)$ component is almost-negligible]. Finally, for the distorted geometry [$R(N–O_{(1)}) = 1.5$ Å], we get the following parameters of the $T_1–S_0$ transition probability: $k^y = 3.77\ s^{-1}$ and $k^z = 4.32\ s^{-1}$, where k^y is the radiative rate constant for the total emission from the T^y spin sublevel (with y- and z-polarization in this case). So the asymmetric vibration ν_3 should strongly influence the $T^y–S_0$ transition intensity and make it comparable with the $T^z–S_0$ transition, while in the ground-state C_{2v} equilibrium geometry, $k^z \gg k^y$ (Table III). This result is in good agreement with the Zeeman-effect study [6] and with the ODMR experiment [7]. Hochstrasser and Marchetti [6] concluded from optical Zeeman data that the T^y spin sublevel is predominantly active in bands of $\nu_{00} + \nu_3' + m\nu_2'$, while the T^z spin sublevel is the most active for ν_2' totally symmetric progression. Comparison of both progressions in ODMR spectra indicates that the non-Condon effects appear to be associated more with the T^z spin sublevel than with the T^y one [7]. From Fig. 5 we can conclude that the M_z transition moment (T^y spin sublevel) is not such a strong function of the bending angle as the M_y transition dipole moment in the important region of ∠ONO variation (up to 125°). M_z is close to zero and crosses the zero line in this region (at ∠ONO = 122.2°), so the $|M_z|^2$ value does not change much at large angles (Fig. 5). The (0–0) band is very weak in both absorption and emission [7] for the T^z and T^y spin sublevels; this means that the ONO angles of about 130° do not contribute much to the transition intensity because of small vibrational overlap for $\nu_2' = \nu_2'' = 0$ bending modes in the ground singlet and in the first excited triplet states. The occurrence of the $\nu_{00} + \nu_3' + m\nu_2'$ progression for the $T_1 \leftarrow S_0$ absorption to the z spin sublevel (and for the corresponding emission) follows from the great enhancement of the $M_y(T^y)$ transition dipole moment upon the asymmetric stretch vibration; the corresponding derivative $dM_y(T^y)/dR$ is estimated to be 0.00144 a.u. This gives

the radiative rate constant for the total emission from the T^y spin sublevel with excitation of one quantum of ν_3 vibration $k^y_{\nu_3} = 1.1\ s^{-1}$. (The vibrational integral $\langle \nu = 0 \mid eQ_3 \mid \nu = 1 \rangle$ is estimated to be 0.183 a.u.) So our estimations of the relative intensities of the $\nu_{00} + \nu'_3 + m\nu'_2$ and $\nu_{00} + m\nu'_2$ progressions seem to agree with the spectra published by Gotberg and Tinti [7].

Nonradiative Processes in Excited States of Nitrite Ions

We wish to comment briefly on the nonradiative processes occurring among the excited states of NO_2^- ions referring to the potentials presented in Figs. 2 and 3 and to the SOC estimations. Hochtrasser and Marchetti [6] first noted that the phosphorescence-to-fluorescence intensity ratio depends on the excitation energy in neat $NaNO_2$ crystals and appears to increase at higher frequencies of exciting photons. Clark and Tinti [23] confirmed this observation and noted that the normalized ODMR signal intensities $\Delta I/I$ in zero field are also excitation energy dependent. These results imply that several channels for intersystem crossing involving different spin sublevels are operative, and their relative contributions are excitation energy dependent [23]. The populating rate to the T^x spin sublevel dominates at 310- and 365-nm excitation. This is induced by direct $^1B_1 \rightsquigarrow {}^3B_1$ intersystem crossing (ISC) promoted by asymmetric stretch vibrations (ν_3) of the b_2 type. The SOC matrix element

$$\langle {}^3B_1\ ({}^3A'')^x | H^x_{soc} | 1^1B_1({}^1A'') \rangle \tag{17}$$

starts to rise very rapidly upon asymmetric stretch distortion. We can see from Fig. 2 that the $^1B_1$ and $^3B_1$ states go to one dissociation limit upon prolongation of the $N–O_{(1)}$ bond. So the energy gap between the S_1 and the T_1 states diminishes upon the asymmetric stretch distortion, which makes the nonradiative process $^1B_1 \rightsquigarrow {}^3B^x_1$ efficient for the phosphorescent T_1 state pumping by the ν_3 vibrations.

When the exciting photon energy exceeds the $S_1(^1B_1)$ threshold by about 1 eV, presumably an additional channel of the T_1 state pumping becomes competitive. In that case excitation into the $^1A_2$ state occurs and produces the increase in phophorescence [6]. A possible explanation for this increase has been proposed by Hochtrasser and Marchetti [6], accounting for the fact that the $^1A_2$ state is directly coupled to the $^3B_1$ state by symmetry consideration. The same T^x spin sublevel should be pumped by this mechanism. Our calculation by the GAMESS code in the T_1 equilibrium geometry ($R = 1.312$ Å, $\angle ONO = 130.56°$) in TZV basis set gives the SOC matrix element

$$\langle {}^3B^x_1 | H^x_{soc} | 1^1A_2 \rangle = -30.6\ cm^{-1} \tag{18}$$

The $^1A_2$ and $^3B_1$ states cross each other at a rather small angle $\angle ONO = 95°$, which is close to the $^1A_2$ state equilibrium. The $^3B_1$ equilibrium geometry is pretty far from it, which favors a large Franck–Condon factor for the $^1A_2 \rightsquigarrow {}^3B^x_1$ transition. (The $^1A_2$ behavior is similar to the $^3A_2$ potential, shown in Fig. 3.) Very high vibrational quanta of the ν_2 mode should be involved in the ISC process $^1A_2 \rightsquigarrow {}^3B^x_1$. At the same time the ODMR signal intensities $\Delta I/I$ should not be changed by this mechanism.

One more mechanism of the ISC process is possible upon $^1A_2$-state excitation. From Fig. 2 we see that the $^1A_2$ and $^3B_2$ states are quite close in energy (0.3 eV; Table II). Their equilibrium positions for ν_2 oscillators are also shifted (Fig. 3). The SOC integral calculated by the GAMESS code in the TZV basis set is

$$\langle {}^3B^y_2 | H^y_{soc} | 1^1A_2 \rangle = -48.5 cm^{-1} \tag{19}$$

As far as the nonradiative transition $^1A_2 \rightsquigarrow {}^3B^y_2$ occurs, a fast internal conversion $^3B^y_2 \rightsquigarrow {}^3B^y_1$ will pump the phosporescent state. In that case the ODMR signal intensities $\Delta I/I$ should depend on the excitation wavelength, as observed by Tinti *et al.*[7,23,24].

The most realistic mechanism of the excitation energy dependence on the phosphorescence-to-fluorescence quantum yield ratio which appears energetically accessible is the one which involves the ISC route $^1B_1 \rightsquigarrow {}^3B_2$. The SOC integral calculated by the GAMESS code in the TZV basis set in the $^1B_1$-state optimized geometry is

$$\langle {}^3B^z_2 | H^z_{soc} | {}^1B_1 \rangle = 10.37\ cm^{-1} \tag{20}$$

It is higher than the corresponding SOC integral (8) for the S–T-interchanged states (in simple approximation [6] such integrals are equal to each other) and it increases upon the asymmetric stretch distortion. From comparison of Figs. 2 and 3 we see that potential energy surfaces of the $^1B_1$ and $^3B_2$ states cross each other at the prolonged $N–O_{(1)}$ bond length and at the same angle which corresponds approximately to the vertical excitation geometry. The phosphorescence-to-fluorescence quantum yield ratio should be changed abruptly when the $^1B_1$- and $^3B_2$-state crossing occurs at a higher excitation energy ($\nu \geq 28000\ cm^{-1}$) [22,24,39]. This does not contradict the ODMR signal intensity $\Delta I/I$ dependence on the excitation wavelength, which was observed by Tinti *et al.* [7,23,24]. The theory of Kokai and Azumi [39], which considers only interplay between the energy-dependent vibrational

relaxation and the $^1B_1 \rightsquigarrow {}^3B_1$ intersystem crossing processes, seems to be incomplete in that respect.

CONCLUSIONS

The results of the present work agree qualitatively with polarization and Zeeman-effect measurements of the $T_1 \leftarrow S_0$ ($^3B_1 \leftarrow 1^1A_1$) transition in absorption of NO_2^- ions in $NaNO_2$ crystals [6] and with ODMR spectra [7] detected by phosphorescence. The T^z spin sublevel has the largest electric-dipole activity and produces y-polarization (Fig. 1, Table III). The corresponding transition moment, denoted M_y in Fig. 5, decreases almost-linearly with an increase in the ONO bond angle in the spectral-important region 110–135°. The anomalous intensity distributions for the progression of the totally symmetric bending mode (ν_2) associated with the T^z spin sublevel (the so-called non-Condon effects in the phosphorescence spectrum and in the cold T ← S absorption of nitrite anions) have been interpreted by Gotberg and Tinti [7] in terms of such linear dependence of the stolen transition moment on the totally symmetric coordinate of the bending mode. At the same time they mentioned that "the detailed mechanism causing this effective linear dependence is unclear" [7]. Our results are complementary to their analysis. The vertical $^3B_1^z \leftarrow 1^1A_1$ transition intensity with z-polarization is very weak (Table III), in agreement with absorption measurements. The difference in the permanent dipole moments of the T_1 and S_0 states in NO_2^- ions is very small in the ground-state geometry. But its contribution to the transition moment Eq. (16) increases with the asymmetric stretch distortion; the involvement of the asymmetric vibration ν_3 should strongly influence the T^y transition intensity. This result is in good agreement with the Zeeman-effect study [6] and with the ODMR experiment [7]. The calculated bending and asymmetric stretch potentials (Figs. 2 and 3) together with the SOC estimations can help to rationalize the nonradiative processes occurring among the excited states of NO_2^- ions. The dependence of the phosphorescence-to-fluorescence intensity ratio on the excitation energy in neat $NaNO_2$ crystals is qualitatively interpreted on this background.

ACKNOWLEDGMENTS

This work was supported by a scholarship (B.F.M.) from Linköping University.

REFERENCES

1. A. Jablonski (1933) *Nature* **131**, 839.
2. A. N. Terenin (1943) *Acta Physicochim. URSS* **18**, 210.
3. S. P. McGlynn, T. Azumi, and M. Kinoshita (1969) *Molecular Spectroscopy of the Triplet State*, Prentice Hall, Englewood Cliffs, NJ.
4. H. J. Maria, A. Wahlborg, and S. P. McGlynn (1968) *J. Chem. Phys.* **49**, 4925.
5. W. Dietrich and D. Schmid (1976) *Phys. Stat. Solid. B* **74**, 609.
6. R. M. Hochstrasser and A. P. Marchetti (1969) *J. Chem. Phys.* **50**, 1727.
7. K. E. Gotberg and D. S. Tinti (1985) *Chem. Phys.* **96**, 109.
8. A. Yamashita and T. Azumi (1984) *J. Phys. Chem.* **88**, 4622.
9. M. I. Kay and B. C. Frazer (1961) *Acta Cryst.* **14**, 56.
10. B. F. Minaev (1976) *Opt. Spectrosc. (USSR)* **41**, 446.
11. S. P. McGlynn (1973) *Bull. Russ. Acad. Sci. Div. Phys. Sci.* **37**, 79.
12. B. F. Minaev, Z. M. Muldahmetov, I. S. Irgibaeva, T. O. Tlepbergenov, and D. M. Kizner (1982) *Int. J. Quant. Chem.* **22**, 863.
13. B. F. Minaev, I. S. Irgibaeva, and Z. M. Muldahmetov (1984) *Teor. Eksp. Khim.* **20**, 305.
14. H. Ågren, O. Vahtras, and B. F. Minaev (1996) *Adv. Quantum Chem.* **27**, 71.
15. M. I. McCarthy, K. A. Peterson, and W. P. Hess (1996) *J. Phys. Chem.* **100**, 6708.
16. N. C. Handy, J. D. Goddard, and H. F. Schaefer III (1979) *J. Chem. Phys.* **71**, 426.
17. L. E. Harris (1973) *J. Chem. Phys.* **58**, 5615.
18. S. J. Strickler and M. Kasha (1963) *J. Am. Chem. Soc.* **85**, 2899.
19. L. E. Rezmik (1978) *Bull. Russ. Acad. Sci. Div. Phys. Sci.* **42**, 27.
20. K. K. Rebane and P. M. Saari (1973) *Bull. Russ. Acad. Sci. Div. Phys. Sci.* **37**, 142.
21. K. K. Rebane and P. M. Saari (1976) *Bull. Russ. Acad. Sci. Div. Phys. Sci.* **40**, 8.
22. I. R. Sildos, L. A. Rebane, and V. E. Peet (1980) *J. Mol. Struct. (TEOCHEM)* **61**, 67.
23. S. E. Clark and D. S. Tinti (1979) *Chem. Phys. Lett.* **60**, 292.
24. S. E. Clark and D. S. Tinti (1980) *Chem. Phys.* **51**, 17.
25. K. E. Gotberg and D. S. Tinti (1982) *Mol. Phys.* **47**, 97.
26. W. C. Allen and R. N. Dixon (1969) *Trans. Faraday Soc.* **65**, 1168.
27. S. R. Langhoff and E. R. Davidson (1976) *J. Chem. Phys.* **64**, 4699.
28. B. F. Minaev (1979) *Fizika Mol. Naukova Dumka Kiev* **7**, 34.
29. B. F. Minaev (1973) *Studies of the Spin-Orbit Coupling Effects in Optical and ESR Spectra of Molecules*, Ph.D. dissertation, Tomsk State University, USSR.
30. O. Vahtras, H. Ågren, P. Jørgensen, H. J. Aa. Jensen, T. Helgaker, and J. Olsen (1992) *J. Chem. Phys.* **97**, 9178.
31. Y. Luo, D. Jonsson, P. Norman, K. Ruud, H. Ågren, B. Minaev, A. Rizzo, and K. V. Mikkelsen (1998) *Int. J. Quant. Chem.* **70**, 219.
32. T. Helgaker, H. J. Aa. Jensen, P. Jøsrgensen, J. Olsen, H. Ågren, K. L. Bak, V. Bakken, K. V. Mikkelsen, P. Norman, K. Ruud, P. R. Taylor, and O. Vahtras (1997) *DALTON, a Second-Order MCSCF Molecular Property Program.*
33. D. E. Woon and T. H. Dunning (1993) *J. Chem. Phys.* **98**, 1358.
34. A. Schafer, H. Horn, and R. Ahlrichs (1992) *J. Chem. Phys.* **97**, 2571.
35. S. E. Clark and D. S. Tinti (1980) *Chem. Phys.* **53**, 403.
36. M. W. Schmidt, K. K. Baldridge, J. A. Boats, S. T. Elbert, M. S. Gordon, J. H. Jensen, S. Koseki, N. Matsunaga, K. A. Nguyen, S. J. Su, and T. L. Windus (1993) *J. Comput. Chem.* **14**, 1347.
37. S. Koseki, M. H. Schmidt, M. S. Gordon, and N. Matsunaga (1995) *J. Phys. Chem.* **99**, 12764.
38. P. J. Hay and T. H. Dunning Jr. (1977) *J. Chem. Phys.* **67**, 2290.
39. F. Kokai and T. Azumi (1982) *J. Phys. Chem.* **82**, 177.